et l'on aura de la même façon:

$$\mathbf{K}^g\mathbf{r}'+(\mathbf{h}-\mathbf{g})\mathbf{r}'-s_g t\simeq\mathbf{k}^h\mathbf{r}' .$$

On obtient deux intégrales ayant la même forme que celle qui vient d'être calculée, d'où le résultat.

APPENDICE 2

ψ_1 s'écrit alors

$$\psi_1=\Sigma'_h(U_h+i\bar{U}_h)$$

$$\times\iint\frac{\exp[2\pi i(\mathbf{r}-\mathbf{r}')\mathbf{k}'].\exp[2\pi i(\mathbf{k}_h+i\mathbf{S}_0/2)\mathbf{r}]}{(2\pi)^3[k'^2-(\mathbf{k}+i\mathbf{S}_0/2)^2]}d\mathbf{k}'d\mathbf{r}' .$$

L'intégration par rapport à dx et dy fournit:

$$\exp(2\pi i)(\mathbf{k}_h+i\mathbf{S}_0/2)\mathbf{r}\sum_h(U_h+i\bar{U}_h)$$

$$\times\iint\frac{\exp[-2\pi i(k_h^z-k'_z)t\,]-1}{(k_{hz}^h-k'_z+iS_{0z}/2)\,(k'^2_z-K_z^{2h}-S_0^2/4+i\mathbf{S}_0\mathbf{k})dk'_z} ,$$

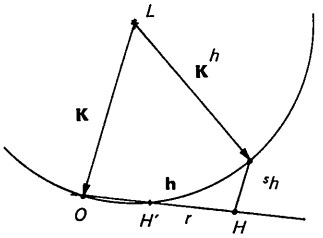

Fig. 5. Définition du vecteur $\mathbf{K}^h$.

puisque le dénominateur prend la forme

$$k'^2-k^2+\frac{S_0^2}{4}+i\mathbf{S}_0\mathbf{k}$$

au degré d'approximation déjà envisagé cette expressions de ψ_1 redonne la valeur précédemment trouvée dans le cas où l'on négligeait l'absorption. En effet le terme $S_0^2/4$ peut être négligé devant $k^2S_0=\bar{U}_0/K=\bar{V}_0/E\lambda_0$ puisqu'il reste voisin de 10^{-3} Å^{-1} pour des électrons d'énergies élevées (100 keV) par exemple, donc est négligeable devant K_{hz} et au même degré d'approximation que précédemment il en est de même de $\mathbf{S}_0\mathbf{k}$ qui est de l'ordre de 10^{-2} Å, on obtient donc l'expression de ψ_1 sans absorption. L'expression de ψ_1 dans le cas des 2 faisceaux sera identique si l'on peut négliger la partie imaginaire de σ donc lorsque $\bar{V}_h\simeq$ 0,1 eV.

Références

FENGLER, H. (1961). *Z. Naturforsch.* **16**a, 1205.
FUJIMOTO, F. (1965). *Z. Naturforsch.* **20**a, 367.
FUJIMOTO, F. (1959). *J. Phys. Soc. Japan.* **14**, 1958.
FUJIWARA, K. (1959). *J. Phys. Soc. Japan.* **14**, 1513.
GEVERS, R. (1963). *Phys. Stat. Sol.* **3**, 1672.
HIRSH, P. B., HOWIE, A., NICHOLSON, R. B., PASHLEY, D. W. & WHELAN, M. J. (1965). *Electron Microscopy of Thin Crystals.* London: Butterworths.
HOERNI, J. A. (1956). *Phys. Rev.* **102**, 1534.
MOTT, N. F. & MASSEY, H. S. W. (1965). *The Theory of Atomic Collisions.* Oxford: Clarendon Press.
NIEHRS, H. & WAGNER, E. H. (1955). *Z. Phys.* **143**, 285.
SMITH, G. H. & BURGE, R. E. (1962). *Acta Cryst.* **15**, 182.
STURKEY, L. (1962). *Proc. Phys. Soc.* **80**, 321.
TOURNARIE, M. (1960). *Bull. Soc. franc. Minér. Crist.* **83**, 179.

Acta Cryst. (1968). A**24**, 513

Magnetic Structure of $Fe_{0.9}Mn_{0.9}Ge$

BY TOSHIRO SUZUOKA*, E. ADELSON,† AND A. E. AUSTIN†
Battelle Memorial Institute, Columbus, Ohio, U.S.A.

(*Received* 25 *July* 1967 *and in revised form* 26 *January* 1968)

The magnetic structure of $Fe_{0.9}Mn_{0.9}Ge$ was studied on a single crystal by neutron and X-ray diffraction. The crystal structure is the hexagonal $B8_2$ and the room temperature data indicated the distribution of metal atoms to be 0·83Mn + 0·12Fe + 0·05 hole in the 2(*a*) site and 0·78Fe + 0·07Mn + 0·15 hole in the 2(*d*) site. Low temperature data at 103 °K were analyzed by assuming a general model, from which four possible structures with non-collinear spins were found. These gave the same net magnetic moment per molecule of 1·66μ_B. Magnetization measurements yielded the Curie point at 241 °K and the moment of 1·39μ_B.

Introduction

The binary systems of 3*d* transition metals with germanium contain phases with the hexagonal $B8_2$ or $D8_8$ type of structure. These structures have two types of site for the transition metal, making layers of transition metal atoms only or transition metal atoms plus germanium atoms. The presence of two metal atom sites offers possibilities of metal ordering in ternary compounds. It has been shown that the $Fe_{1.67}Ge$ compound has the $B8_2$ crystal structure while the Mn_5Ge_3 compound has the related $D8_8$ crystal structure. Both compounds have ferrimagnetic structures (Ciszewski, 1963; Adelson & Austin, 1965). As part of our research on

* IAEA Fellow from the Research Institute for Iron, Steel and Other Metals, Tohoku University, Sendai, now at the Department of Electrical Engineering, Faculty of Engineering, Yamaguchi University, Ube, Japan.
† Battelle Memorial Institute, Columbus Laboratories, Columbus, Ohio, U.S.A.

these systems, we have investigated the ternary system Fe–Mn–Ge. The present study is on the crystal and magnetic structure of the ternary compound $Fe_{0\cdot9}Mn_{0\cdot9}Ge$.

Experimental procedure

Materials were prepared by the method described in a previous paper (Adelson & Austin, 1965). The composition $Fe_{0\cdot9}Mn_{0\cdot9}Ge$ forms a continuous solid solution with $Fe_{1\cdot67}Ge$, with the hexagonal $B8_2$ crystal structure, $P6_3/mmc$ (D^4_{6h}). This was shown by examination of several compositions $(Fe_{1-x}Mn_x)_{1\cdot67}Ge$ with $x=0\cdot2$, $0\cdot4$, $0\cdot5$, $0\cdot6$ and for FeMnGe. The last three compositions had second phases of $FeGe_2$, Mn_5Ge_3, Fe_3Ge, respectively. The lattice constants for $Fe_{0\cdot9}Mn_{0\cdot9}Ge$ determined by powder X-ray diffraction with Fe $K\alpha$ radiation were $a_0=4\cdot088\pm0\cdot002$ and $c_0=5\cdot184\pm0\cdot002$ Å. The pycnometric density of the ingot was $7\cdot668\pm0\cdot005$ g.cm^{-3}. This measured density gave $Z=2\cdot01$ for the molecular weight of $Fe_{0\cdot9}Mn_{0\cdot9}Ge$. The close agreement to the theoretical value $Z=2$ indicated metal site vacancies instead of excess Ge atoms substituting in the metal sites. The population of these vacancies in the (a) and (d) sites was determined by powder X-ray diffraction with Fe $K\alpha$ from the intensity ratios observed for 00.2/00.4, 10.0/30.0, 10.1/20.2, 10.0/11.0, and 10.1/11.0. These ratios are not affected by preferred orientation. The occupancy fraction of vacancies was found to be $0\cdot05\pm0\cdot05$ in the 2(a) site and $0\cdot15\pm0\cdot05$ in the 2(d) site. In the intensity calculation, the two kinds of metal atoms were assumed to have the same X-ray scattering factor.

Neutron diffraction data were obtained on diffractometers at the Battelle Research Reactor using a monochromated beam with 1·04 Å wavelength. Measurements were made at room temperature and 103°K. A single crystal $3\times4\times5$ mm in size was used. This crystal showed practically no extinction effects. Magnetization was measured on a pendulum magnetometer at an applied field of 12 kilogauss from room temperature to 77°K.

Neutron diffraction at room temperature

There are only nuclear scattering contributions to the neutron diffraction intensities of $Fe_{0\cdot9}Mn_{0\cdot9}Ge$ at room temperature. Fig. 1 shows that the magnetic 00.1 peak intensity decreases with increasing temperature and disappears above 213°K. The intensities of twenty reflections were analyzed after elimination of a small contamination due to the half-wavelength. The results indicated ordering in the distribution of Fe and Mn atoms in the metal sites. Fig. 2 shows the comparison of the observed intensities with the calculated $I(hk.l)/I(11.0)$ as a function of the fraction of Fe atoms in the 2(d) site. The Debye temperature Θ was assumed to be 425°K, a value suggested by that of $Fe_{1\cdot60}Ge$ (Adelson & Austin, 1965). The results indicate that almost all Fe atoms occupy the 2(d) sites and almost all Mn atoms occupy the 2(a) sites. The best fit was obtained with the following distribution:

	Hole	Fe	Mn
2(a) site	0·05	0·12	0·83
2(d) site	0·15	0·78	0·07

With this distribution the Debye temperature was redetermined from the slope of $\ln(I_{obs}\sin 2\theta/F^2_{0calc})$

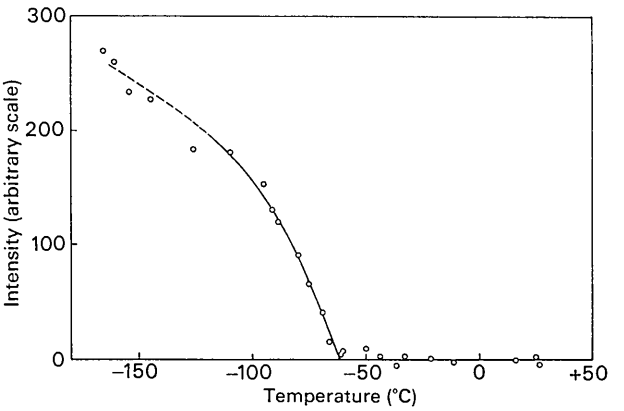

Fig. 1. Variation of the peak intensity of 00.1 of $Fe_{0\cdot9}Mn_{0\cdot9}Ge$ with temperature.

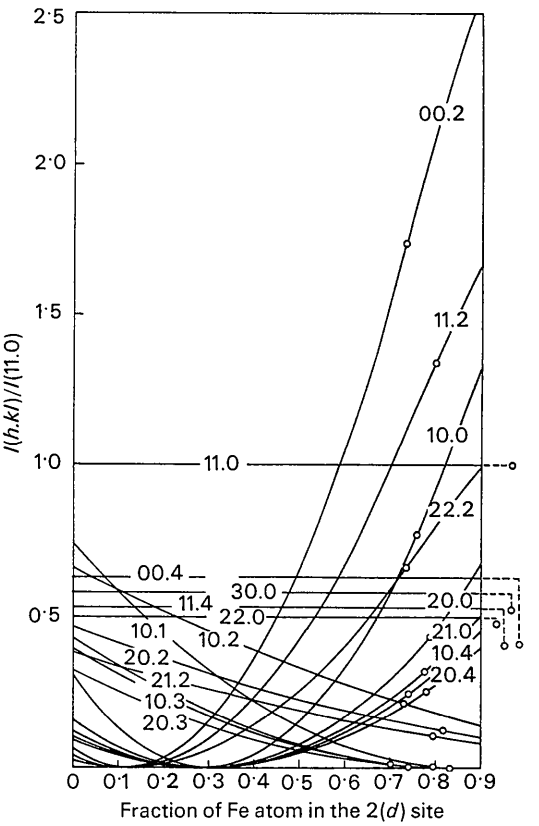

Fig. 2. Nuclear scattering intensities of $Fe_{0\cdot9}Mn_{0\cdot9}Ge$ as a function of the atomic fraction of Fe in the 2(d) site, calculated (curves) and observed (circles).

with respect to $(\sin\theta/\lambda)^2$, where θ is the Bragg angle, F_0 is the structure amplitude factor disregarding thermal motions, and λ is the neutron wavelength. The value of Θ thus obtained was 400 ± 130°K. The recalculation using this value had little effect on the distribution concluded above. Table 1 gives the theoretical and experimental values of F_0^2 at room temperature.

Table 1. *Nuclear scattering intensities of* $Fe_{0.9}Mn_{0.9}Ge$ *(at room temperature)*

hk.l	F_0^2calc	F_0^2obs
00.1	0	0
00.2	12·11	11·10
00.3	0	0
00.4	7·62	5·36
10.0	3·69	3·64
20.0	3·69	4·14
30.0	7·62	7·55
10.1	0·0432	0·0452
10.2	1·44	1·71
10.3	0·0432	0·128
10.4	3·69	3·39
20.1	0·0432	0·0192
20.2	1·44	1·38
20.3	0·0432	0·0695
20.4	3·69	4·08
21.0	3·69	4·02
21.1	0·0432	–
21.2	1·44	1·51
21.3	0·0432	–
11.0	7·62	8·21
11.1	0	0
11.2	12·11	14·03
11.3	0	–
11.4	7·62	6·28
22.0	7·62	7·92
22.1	0	–
22.2	12·11	11·78

Magnetic structure

Low temperature measurements were made at 103°K by using a cryostat of aluminum. The scattering due to the wall of the aluminum vessel was eliminated by blank measurements for each diffraction line. Intensities of the magnetic scattering were obtained for fourteen reflections. Only reflections with strong magnetic intensities but with weak or zero nuclear intensities were analyzed. Those were 00.1, 00.3, 10.1, $\bar{1}$0.1, 10.2, 10.3, $\bar{1}$0.3, 20.1, 20.2, 20.3, and 11.1. The 00.2 intensity was added to them because it is least affected by any uncertainty in the form factor. The other two, 10.0 and 11.0, were for reference only. The form factor, $Fe\overline{f(d)}$, obtained by Weiss & Freeman (1959), was used both for Fe and Mn atoms.

The magnetic structure was proposed with no special assumption except that there are non-collinear spins in order to account for the 00.1, 00.3, and 11.1 reflections. When the Debye temperature factor is omitted, the magnetic structure factor in the full vector expression is given by

$$\mathbf{q}F=\sum_i \mathbf{p}_i \sin\alpha_i \exp(i\psi_i)\exp(i\boldsymbol{\tau}\cdot\mathbf{r}_i),$$

where $\mathbf{q}$ is the magnetic interaction vector, $\mathbf{p}_i$ is the magnetic amplitude vector of the ith atom, α_i is the angle between the spin vector and the scattering vector, ψ_i is the phase angle of the spin vector in the reflection plane, $\boldsymbol{\tau}$ is the reciprocal lattice vector for the reflection, and $\mathbf{r}_i$ is the position vector of an atom. For simplicity, we take $\mathbf{p}_i$ to be the spin vector itself omitting the form factor, $f(\overline{d})$, and write the corresponding magnetic structure factor by $\mathbf{q}F_0$. The spin vector $\mathbf{p}_i$ can be resolved into the two components, $\mathbf{p}_i^c$ and $\mathbf{p}_i^b$, respectively, parallel and perpendicular to the c axis. The phase angle ψ_i is also replaced by η_i and φ_i, where η_i is the phase angle along the c axis, so that it must be 0 or π, while φ_i is the phase angle in the basal plane. Thus

$$\mathbf{q}F_0=\sum_i \mathbf{p}_i^c \sin\alpha_i^c \exp(i\eta_i)\exp(i\boldsymbol{\tau}\cdot\mathbf{r}_i)+\sum_i \mathbf{p}_i^b \sin\alpha_i^b \exp(i\varphi_i)\exp(i\boldsymbol{\tau}\cdot\mathbf{r}_i),$$

where α_i^c and α_i^b are the angles between the scattering vector and the spin component vector along and perpendicular to the c axis, respectively. Then we have

$$q^2F_0^2=\sum_i\sum_j p_i^c p_j^c \sin\alpha_i^c \sin\alpha_j^c \cos(\eta_{ij}+R_{ij})+\sum_i\sum_j p_i^b p_j^b \sin\alpha_i^b \sin\alpha_j^b \cos(\varphi_{ij}+R_{ij}),$$

where

$$\eta_{ij}=\eta_i-\eta_j,\ \varphi_{ij}=\varphi_i-\varphi_j,\ \text{and}\ R_{ij}=\boldsymbol{\tau}\cdot(\mathbf{r}_i-\mathbf{r}_j).$$

The average over the possible domains gives

$$q^2F_0^2=\sin^2\Phi\sum_i\sum_j p_i^c p_j^c \cos\eta_{ij}\cos R_{ij}+\tfrac{1}{2}(1+\cos^2\Phi)\sum_i\sum_j p_i^b p_j^b \cos\varphi_{ij}\cos R_{ij},$$

where Φ is the angle between $(hk.l)$ and the basal plane.

From the distribution concluded previously, we assume that Mn atoms occupy only the 2(a) sites and Fe atoms occupy only the 2(d) sites. We further assume $\varphi_1=-\varphi_2$ for the 2(a) site and $\varphi_3=-\varphi_4$ for the 2(d) site because of ordering. Since we can take $\eta_1=0$, we have eight possible cases for the combinations of η's as follows:

	(i)	(ii)	(iii)	(iv)	(v)	(vi)	(vii)	(viii)
η_1	0	0	0	0	0	0	0	0
η_2	0	0	0	π	0	π	π	π
η_3	0	0	π	0	π	0	π	π
η_4	0	π	0	0	π	π	0	π

The value of $\cos\eta_{ij}$ $(i\neq j=1,2,3,4)$ is either $+1$ or -1. Thus, since Φ and R_{ij} are known quantities in the equation above, it is possible to solve for the unknown $p_1=p_2=p_a$, $p_3=p_4=p_d$, φ_1 and φ_3, for example, in cases (i) and (v) which give the same expressions,

$$q^2F_0^2(00.1)=0+[4(p_a^b\sin\varphi_1)^2+4(p_d^b\sin\varphi_3)^2]$$
$$q^2F_0^2(10.0)=[4(p_a^c\pm p_d^c)^2]+0{\cdot}500[4(p_a^b\cos\varphi_1+p_d^b\cos\varphi_3)^2],\ \textit{etc.}$$

where the first term in brackets is the c-axis term and the second term is the basal component.

The expressions for 10.1, 10.3, 20.1, and 20.3 involve multiples of $3(p_d^c)^2$ and $4(p_a^b \sin\varphi_1)^2+3(p_d^b \cos\varphi_3)^2+(p_d^b \sin\varphi_3)^2$. Thus, these terms can be determined by least-squares calculations of observed intensity data. The results are:

$$(p_d^c)^2 = -0{\cdot}07 \pm 0{\cdot}14$$

and

$$4(p_a^b \sin\varphi_1)^2+3(p_d^b \cos\varphi_3)^2+(p_d^b \sin\varphi_3)^2 = +1{\cdot}21 \pm 0{\cdot}43 .$$

Since $(p_d^c)^2$ must be positive, we can conclude that $p_d^c=0$. [Similar situations occur in all other cases, although $3(p_d^c)^2$ is replaced by $(p_d^c)^2$ in cases (ii) and (iii), by $4(p_a^c)^2+(p_c^c)^2$ in (vi) and (vii), and by $(2p_a^c \pm \sqrt{3}p_d^c)^2$ in (viii) and (iv).]

Assuming $p_d^c=0$, we then have as the final forms of equations to be solved

00.1, 00.3, 11.1: $4[(p_a^b \sin\varphi_1)^2+(p_d^b \sin\varphi_3)^2]=0{\cdot}98$

10.1, 10.3, 20.1, 20.3: $4(p_a^b \sin\varphi_1)^2+3(p_d^b \cos\varphi_3)^2+(p_d^b \sin\varphi_3)^2=1{\cdot}02$

10.2: $1{\cdot}40(p_a^c)^2+0{\cdot}826[(2p_a^b \cos\varphi_1+p_d^b \cos\varphi_3)^2+3(p_d^b \sin\varphi_3)^2]=0{\cdot}56$

20.2: $2{\cdot}72(p_a^c)^2+0{\cdot}661[(2p_a^b \cos\varphi_1+p_d^b \cos\varphi_3)^2+3(p_d^b \sin\varphi_3)^2]=0{\cdot}60$

00.2: $4[(p_a^b \cos\varphi_1+p_d^b \cos\varphi_3)^2]=0{\cdot}80$.

It should be noted that the observed value of 0·98 for 00.1, 00.3, and 11.1 is the mean value in consideration of experimental weights and the value 1·02 for 10.1, 10.3, 20.1, and 20.3 is recalculated again by the least-squares method by assuming no component along the c axis of the 2(d) site spin.

Now the subsequent procedure is purely mathematical. A remarkable result, $(p_d^b \cos\varphi_3)^2 \simeq (p_d^b \sin\varphi_3)^2$, is obtained by substituting the first equation from the second, giving $\varphi_3 = \pm 45°$ or $\pm 135°$. We find that these lead to the same solutions. They are given as solutions I and II in Table 2, where the β's are the angles of the spins from the c axis, the p's are the effective scattering amplitudes in 10^{-12} cm, μ_a and μ_d are the magnetic moments per atom in the respective sites in Bohr magnetons taking account of the population in metal sites, and μ_{net} is the effective ferromagnetic moment per molecule $Fe_{0.9}Mn_{0.9}Ge$ in Bohr magnetons. μ_{net} is given by the following relation:

$$\begin{aligned}\mu_{net} &= \tfrac{1}{2}|0{\cdot}95\{(\boldsymbol{\mu}_a)_1+(\boldsymbol{\mu}_a)_2\}+0{\cdot}85\{(\boldsymbol{\mu}_d)_3+(\boldsymbol{\mu}_d)_4\}| \\ &= \tfrac{1}{2}[(2p_a^c+2p_d^c)^2+(p_a^b \sin\varphi_1+p_a^b \sin\varphi_2+p_d^b \sin\varphi_3 \\ &\quad +p_d^b \sin\varphi_4)^2+(p_a^b \cos\varphi_1+p_a^b \cos\varphi_2+p_d^b \cos\varphi_3 \\ &\quad +p_d^b \cos\varphi_4)^2]^{1/2}/(e^2\gamma/2mc^2) ,\end{aligned}$$

where e and m are the electron charge and mass, respectively, c is the velocity of light, and γ is the magnetic moment of the neutron expressed in nuclear magnetons. It is noted that in this equation $\varphi_1=-\varphi_2$ and $\varphi_3=-\varphi_4$ and the factor $\frac{1}{2}$ enters because of the presence of two molecules in the unit cell.

Table 2. *Magnetic structure of* $Fe_{0.9}Mn_{0.9}Ge$

Model		I	II	III	IV
2(a) site	μ_a	1·73	2·72	0·82	2·60
	β_a	46°	64°	90°	90°
	$\varphi_{1,2}$	±102°	±128°	±90°	±132°
	$p_a{}^c$	0·31	0·31	0	0
	$p_a{}^b$	0·32	0·62	0·21	0·67
2(d) site	μ_d	2·36	0·38	2·75	0
	β_d	90°	90°	90°	90°
	$\varphi_{3,4}$	±45°	±45°	±45°	—
	$p_d{}^c$	0	0	0	0
	$p_d{}^b$	0·54	0·09	0·63	0
	μ_{net}	1·66	1·66	1·66	1·66

β's are angles from the c axis.

Solutions I and II also occur in cases (ii) and (iii) where similarly $p_d^c=0$. Solutions III and IV in Table 2 are derived from cases (iv), (vi), (vii), and (viii) where $p_a^c=p_d^c=0$.

In the above calculations, the most general expressions for $q^2F_0^2$ are employed. Any more reflection measurements only offer less accurate data because of the uncertainty in the form factor in high angle reflections. The analytical method used is quite general except for the assumption that $p_d^c=0$ or $p_a^c=p_d^c=0$, the validity of which depends on the experimental accuracy, but the actual structure should not be far from either one found here. Table 3 gives the values of $q^2F_0^2$ calculated and observed.

Table 3. *Magnetic intensities* $q^2F_0^2$ *of* $Fe_{0.9}Mn_{0.9}Ge$

	Model		
hk.l	I & II	III & IV	Obs.
00.1	0·98	0·98	0·99
00.3	0·98	0·98	0·52
11.1	0·56	0·56	0·64
00.2	0·80	0·80	0·80
10.1	0·67	0·67	0·70
10.3	0·92	0·92	0·62
20.1	0·56	0·56	0·32
20.3	0·77	0·77	1·00
10.2	0·56	0·65	0·56
20.2	0·60	0·52	0·60
10.0	0·73	0·40	0·27
11.0	0·59	0·40	1·83

Magnetization measurements

Fig. 3 shows the magnetization data (σ gram) of $Fe_{0.9}Mn_{0.9}Ge$ from room temperature to 77 °K (liquid nitrogen temperature) at an applied field of 12 kilogauss. The Curie temperature was found to be 241 °K according to a linear plot of σ^2 *versus* temperature. The magnetization of 45 emu.g^{-1} at liquid nitrogen temperature yielded 1·39μ_B per molecule which is in agreement with the value of 1·66μ_B obtained from the neutron diffraction data. Above the Curie point the

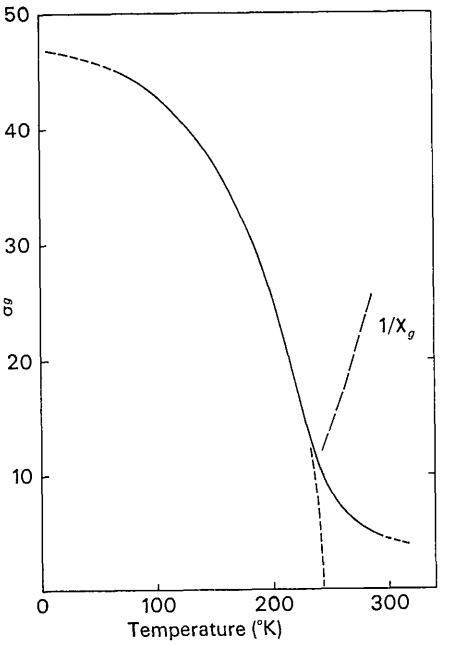

Fig. 3. Magnetization (σ gram) and $1/\chi_g$ of $Fe_{0\cdot9}Mn_{0\cdot9}Ge$ at 12 kilogauss.

calculated inverse susceptibility per gram, $1/\chi_g$, is also shown, although the temperature range is not wide enough for calculation of the slope.

Discussion

We have found four possible magnetic structures for $Fe_{0\cdot9}Mn_{0\cdot9}Ge$ from the neutron diffraction data, although we cannot resolve them by the available data. However, by considering their relation to the structures of the binary compounds, Mn_5Ge_3 (Ciszewski, 1963) and $Fe_{1\cdot77}Ge$ (Adelson & Austin, 1965), it can be seen that the most probable structure is the one corresponding to model II. In this model, the moments per metal atom in the respective sites are $\mu_a=2\cdot72$ and $\mu_d=0\cdot38$. Noting that the metal atom distribution is $0\cdot83Mn+0\cdot12Fe$ in site (a) and $0\cdot78Fe+0\cdot07Mn$ in site (d), we can take the (a) sublattice as Mn atoms and the (d) sublattice as Fe atoms, as in the magnetic analysis, and take $2\cdot72\mu_B$ as the moment per Mn atom and $0\cdot38\mu_B$ as the moment per Fe atom. The former moment has a c component while the latter lies in the basal plane with a cant angle $\pm45°$. On the other hand, in terms of the notation in the present paper the Mn_5Ge_3 structure has $\mu_a=3\cdot00$, $\mu_d=2\cdot00$, $\mu_{net}=2\cdot5$, $\varphi_1=\varphi_3=0°$, $\beta_a=\beta_d=0°$ (spins parallel to the c axis) and the $Fe_{1\cdot77}Ge$ structure has $\mu_a=1\cdot30$, $\mu_d=1\cdot10$, $\mu_{net}=1\cdot17$, $\varphi_1=0°$, $\varphi_3=28°$, $\beta_a=\beta_d=90°$ (spins in the basal plane, including (d) site spins with a cant angle $\pm28°$ from the common ferromagnetic components). Therefore, the spin structure of $Fe_{0\cdot9}Mn_{0\cdot9}Ge$ would resemble the structures of both of these binary compounds, that is, the suggested structure has the sublattice (a) similar to Mn_5Ge_3 in magnitude of moment, with a component along the c axis, while the sublattice (d) has low moments with canted directions in the basal plane, comparable with the (d) sublattice of $Fe_{1\cdot77}Ge$. Although these considerations do not exclude the other solutions, they do indicate greater disparity with the binary compounds.

The authors wish to thank Mr J. W. Moody for synthesis of materials, and Mr N. A. Richard for magnetization measurements.

References

ADELSON, E. & AUSTIN, A. E. (1965). *J. Phys. Chem. Solids*, **26**, 1795.
CISZEWSKI, R. (1963). *Phys. Stat. Sol.* **3**, 1999.
WEISS, R. J. & FREEMAN, A. J. (1959). *J. Phys. Chem. Solids*, **10**, 147.

Acta Cryst. (1968). A**24**, 517

Application de la Théorie Dynamique de S. Takagi au Contraste d'un Défaut Plan en Topographie par Rayons X. I. Faute d'Empilement

PAR A. AUTHIER ET D. SIMON

Laboratoire de Minéralogie-Cristallographie associé au C.N.R.S., Faculté des Sciences de Paris, 1, rue Victor Cousin, Paris 5e, France

(*Reçu le* 1 *mars* 1968)

Takagi's dynamical theory of X-ray diffraction by a perfect crystal is described for the two cases of an incident plane-wave and a spherical wave. Emphasis is put on the relation between these two cases. This theory is then applied to a single stacking-fault in a perfect crystal and the same relation is found between the plane-wave case and the spherical wave case. This relation enables us to calculate easily the stacking-fault fringe contrast by the stationary phase method.

1. Introduction

Le contraste de l'image d'un défaut plan a été étudié il y a plusieurs années déjà dans le cas de la microscopie électronique (Whelan & Hirsch, 1957*a*,*b*; Hashimoto, Howie & Whelan, 1960, 1962; Gevers, Van Landuyt & Amelinckx, 1965, 1966).

Le calcul en est simplifié dans une certaine mesure par le fait que l'onde incidente est plane et que l'on peut utiliser l'approximation dite de la colonne. Il est